Organic Synaptic Diodes Based on Polymeric Mixed Ionic-Electronic Conductors

Fabian Gärisch, Giovanni Ligorio,* Patrick Klein, Michael Forster, Ullrich Scherf, and Emil J. W. List-Kratochvil*

Neuromorphic devices are likely to be the next evolution of computing, allowing to implement machine learning within hardware components. In biological neural systems, learning and signal processing are achieved by communication between neurons through time-dependent ion flux in the synapses. Integrating such ion-mediated operating principles in neuromorphic devices can deliver an energy efficient and powerful technology. Here a device known as a light-emitting electrochemical cell is revisited and modified, exploiting its ability to modulate current through ion accumulation/depletion at the electrodes and turn it into an organic synaptic diode. This two-terminal device is based on an organic mixed ionic-electronic conducting polymer that serves as active layer for conduction of lithium ions as well as charge carriers. The ionic conduction properties are modified by cryptand molecules, able to reversibly capture ions. The device can be reliably switched between states for at least 100 cycles and displays state retention for multiple minutes. The applicability for neuromorphic applications is further demonstrated by exploring frequency-dependent plasticity and paired-pulse facilitation behavior in the millisecond range. The polymeric nature, combined with the simple two-terminal architecture of the presented neuromorphic device, opens up a range of possibilities regarding the fabrication of artificial neural networks.

F. Gärisch, G. Ligorio, E. J. W. List-Kratochvil
Humboldt-Universität zu Berlin, Institut für Physik
Institut für Chemie
IRIS Adlershof
Zum Großen Windkanal 2, 12489 Berlin, Germany
E-mail: giovanni.ligorio@hu-berlin.de; emil.list-kratochvil@hu-berlin.de
P. Klein,[+] M. Forster, U. Scherf
Department of Chemistry and Wuppertal Center for Smart Materials
and Systems CM@S
Wuppertal University
Gauss-Str. 20, 42119 Wuppertal, Germany
E. J. W. List-Kratochvil
Helmholtz-Zentrum Berlin für Materialien und Energie GmbH
Hahn-Meitner-Platz 1, 14109 Berlin, Germany

[+]Present address: CAT Catalytic Center, ITMC, RWTH Aachen University, Worringerweg 2, 52074 Aachen, Germany

1. Introduction

The rapid evolution of artificial intelligence—well established at the software level—is pushing the development of devices able to integrate—at the hardware level—the learning capability of biological nervous systems.[1–3] In order to reproduce the functionalities of biological neural networks—based on neurons interconnected through synapses[4]—these systems are mimicked in the form of artificial neural networks (ANNs). Neuromorphic devices serve as building blocks for ANNs, by operating as artificial neurons or synapses. Since the signal transfer across the biological synapse is modulated by ion dynamics, a biomimetic artificial synapse would therefore benefit from imitating this behavior.

This approach has previously been explored and reported in literature, employing mainly transistor-based architectures. There, the conductivity is mediated by ionic doping of the transistor channel.[5,6] While these devices display a variety of neuromorphic functionalities, their architecture is based on three-terminal devices. This approach not only impedes dense integration into ANNs—in the form of crossbar arrays[7]—but also breaks with the biomimetic principle, as the synapse is inherently two-terminal. Thus, an equally two-terminal synaptic device would be preferable and various concepts have been presented in literature. These devices are based on metallic filament formation,[8–10] phase change,[11,12] spin state,[13,14] ferroelectric effects,[15,16] redox chemistry,[17] or biomembranes.[18,19] In this work, we propose to add another mechanism—inspired by the ion-based operating principle of the biological synapse—by revisiting a concept for a wholly different category of device. Although not for neuromorphic applications, controlling the electronic properties of a two-terminal device through dynamic polarization of ions has previously been employed in light-emitting electrochemical cells (LECs).[20,21] In such a device, a single layer, based on an organic mixed ionic-electronic conductor—mixed with a salt—is sandwiched between two electrodes. Upon applying a bias, the salt dissociates and ions drift toward the electrodes, resulting in the formation of electric double layers at the electrode interfaces.[22–25] This allows for improved carrier injection without the need of additional injection or transport layers and upon balanced

injection of charges efficient light emission is observed. This effect is dependent on the concentration of salt in the device. A low salt content prevents efficient injection, while high salt concentrations can lead to adverse effects, such as the formation of separate salt domains.[26,27] A critical point in the device operation of the LEC is that the switch-on time is limited by the ion drift velocity.[28] This intrinsic latency, although small, is unwanted for display applications. However, for the above-discussed neuromorphic applications the ionic modulation of current over time is a highly desirable feature. Additionally, the well-established operation principles of bulk and interface doping in LECs[22–25] are considered an ideal starting point for using this device.

Thus, we propose and demonstrate an artificial neuromorphic device based on a polymer mixed ionic-electronic conductor in which ions are used to modulate the conductive state of the device. For this, ad hoc synthesized polyfluorene was functionalized with tetraethylene glycol (TEG) side chains to improve (lithium) ion conduction. In order to physically limit the movement of ions, prolongating ion polarization times and hence increasing the retention time, a cryptand molecule was dispersed into the polymer layer.[29,30] To the best of our knowledge, the device proposed here is the first two-terminal organic synaptic diode that is able to mimic neuromorphic functions—such as short-term plasticity—through ion-induced modulation of carrier injection, opening up new routes toward the fabrication of artificial neural networks.

2. Results and Discussion

Poly[9,9-bis(3,6,9,12-tetraoxatridecyl)fluorene-2,7-diyl] (TEG-PF) was generated in a Yamamoto-type homocoupling procedure of the respective 2,7-dibromofluorene monomer with Ni(cyclooctadiene)$_2$ as reductive coupling agent.[31,32] High molecular weight TEG-PF was isolated with average molecular weights of M_n 91.3 and M_w 188 kg mol^{-1} (see the Supporting Information).
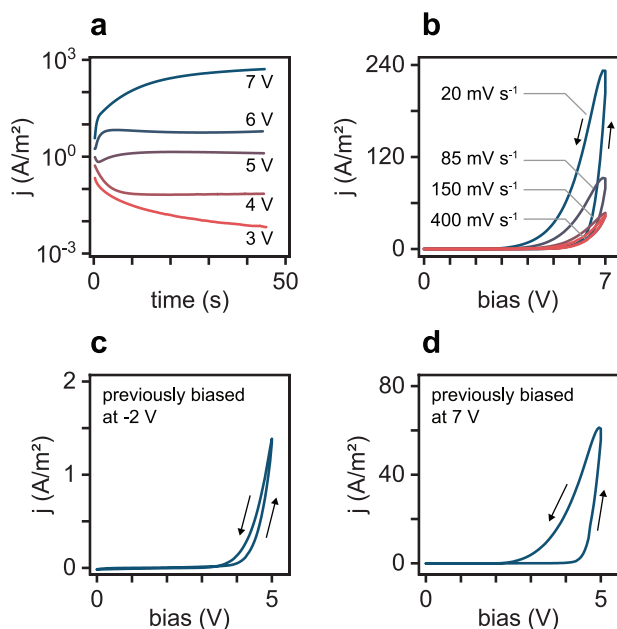
The devices were fabricated on glass coated with prepatterned indium tin oxide (ITO) electrodes (first electrode). The active material was deposited via spin coating from a solution of TEG-PF, [2.2.2]-cryptand, and lithium triflate (LiOTf) dissolved in tetrahydrofuran (THF), forming a layer with a thickness of 200 nm. The second electrode was fabricated by thermal evaporation of aluminum, resulting in an active device area of 2 mm by 2 mm. **Figure 1**a schematically depicts the device architecture. The main component in the active material—TEG-PF—is a semiconducting polyfluorene (PF) functionalized with TEG side chains to improve cation conduction. The polymer chemical structure is displayed in the top part of Figure 1b. To tune the cation conducting properties of the TEG-PF matrix, the bicyclic complexing agent [2.2.2]-cryptand was added. The bottom part of Figure 1b shows its chemical structure.

Cryptands form strong supramolecular assemblies, in which alkali metal ions such as Li$^+$, Na$^+$, and K$^+$ are trapped within the molecule due to chelating effects.[29] This ion trapping is a reversible process,[33] as the cryptand-bound ions are released upon applying an electric potential exceeding a threshold. Lithium triflate salt was added in the active material solution to serve as source for Li$^+$ ions. The large and stable triflate counter ion allows the salt to dissociate in the polymer matrix, releasing free Li$^+$ ions.[34] Cryptand molecules and Li$^+$ ions can be assumed to be dispersed throughout the active layer, as schematically represented in Figure 1c. The weight ratio (4:1:1) between the components results in a stoichiometric excess of Li$^+$ ions compared to cryptand molecules. This ensures the presence of both trapped and free Li$^+$ ions within the active layer. No obvious signs of strong phase separation have been observed.[35]

A positive bias applied to the ITO electrode induces a drift of Li$^+$ ions toward the Al electrode (connected to ground). If the bias is below the threshold voltage, free Li$^+$ ions move, accumulating at the Al electrode. This is schematically depicted in Figure 1d. Exceeding the threshold voltage causes detrapping of Li$^+$ ions bound to the cryptand. Both trapped and free Li$^+$ ions are thus conducted toward the Al electrode, further depleting
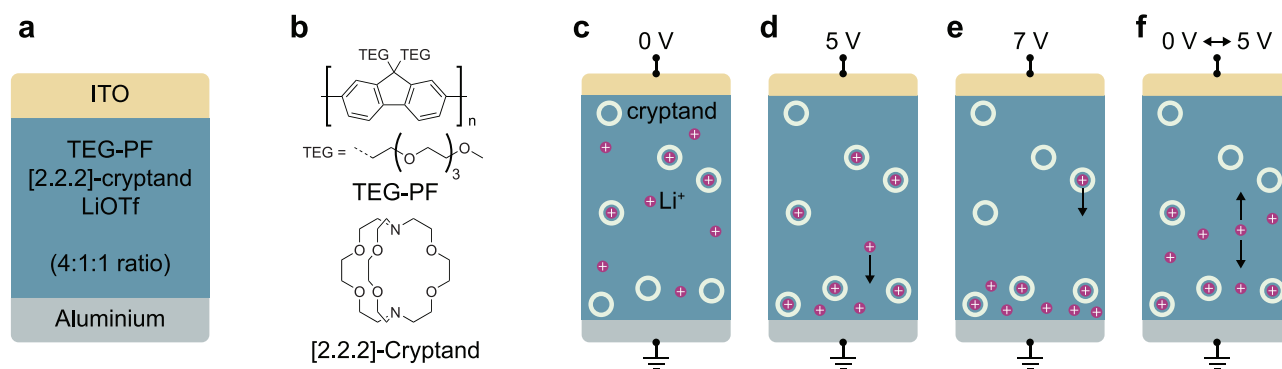
Figure 1. a) The device consists of an ITO anode, active layer, and Al cathode (2 mm by 2 mm). The active layer is a blend of TEG-PF polymer with [2.2.2]-cryptand and LiOTf salt. b) TEG-PF is a mixed ionic-electronic conductor, allowing for a high Li$^+$ ion mobility, while [2.2.2]-cryptand captures and stabilizes Li$^+$ ions. c) Free and cryptand-bound Li$^+$ ions are dispersed through the active material. d) Applying a bias below the threshold leads to a drift of free Li$^+$ ions toward the Al cathode, while cryptand-bound Li$^+$ ions are immobile. e) At a bias above the threshold, previously cryptand-bound ions are mobilized and drift toward the Al cathode. The distribution of cryptand-bound ions is shifted toward the cathode. f) With Li$^+$ ions accumulated at the Al cathode, the device is now prebiased. Free Li$^+$ ions remain mobile and can be shifted with by controlling the bias.

**ADVANCED
SCIENCE NEWS**
www.advancedsciencenews.com

**ADVANCED
ELECTRONIC
MATERIALS**
www.advelectronicmat.de

Figure 2. a) A series of constant bias measurements show the operating range of the device and dynamic behavior over time. b) With decreasing sweep speed, the current and hysteresis increase. c) If previously biased at −2 V, a low current is retained during a sweep to 5 V. d) Conversely, if previously biased at 7 V, the current during a sweep to 5 V is increased more than 40-fold.

the region close to the ITO electrode (see Figure 1e). If the bias is removed, the free Li⁺ ions diffuse (due to higher concentration and self-repulsion) from the Al electrode, while trapped ions remain (Figure 1f). The drift direction of free Li⁺ ions is controlled by inverting the polarity of the applied bias. However, the Al electrode undergoes oxidation if the bias applied is lower than approximately −2 V.[25] As a consequence of the ion concentration at the electrodes, the injection of electric carriers is modulated, thus allowing control over the current through the device,[22–25] as we have previously observed in LECs[36] and LEDs using an anionic conjugated polymer.[37]
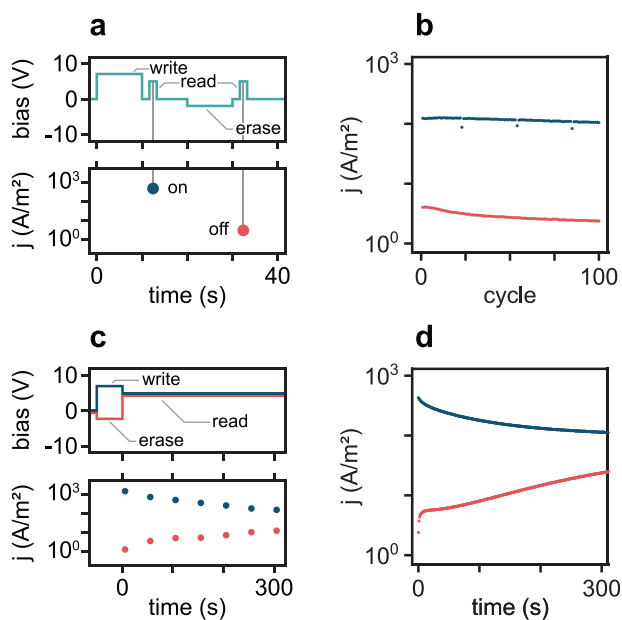
In order to employ the two-terminal device for neuromorphic applications, its electronic behavior was investigated. First, the current density over time was measured as a function of a constant bias applied between the electrodes (between 3 and 7 V). The results of the measurements are reported in **Figure 2**a. The evolution of current density over time displays two different behaviors. In the first part of the evolution, the current results from the superposition of ionic and carrier current. Once the ions are polarized—induced by the applied bias—a second behavior occurs, where the stationary ions no longer contribute to the current. With the exception of the current measured at 7 V, the saturation condition is reached within the first 10 s. This indicates that below 7 V, the ionic current is due to the free Li⁺ ions. At 7 V, the Li⁺ ions bound to the cryptand are detrapped, hence further increasing the ion concentration at the Al electrode and decreasing the ion concentration at the ITO electrode, respectively. This results in an improved injection manifested in increasing current over time. As an effect of the improved injection, light emission becomes visible at above 7 V, as was expected for a device based on an

LEC. Since this voltage regime is beyond the operating range for this device and light emission was weak, light-based neuromorphic functionality was not further investigated. Reference devices without cryptand addition showed light emission at a lower voltage (above 4 V), corresponding to a higher current measured in comparison to the devices containing cryptand (see Figure S4, Supporting Information).

Given the fact that the current is influenced by the ion concentration at the electrodes, it is expected that the current density versus applied bias (J–V) characteristic is influenced by the sweep speed (the speed at which the bias sweep occurs). In order to verify how the latter influences the J–V curve, measurements with increasing sweep speed were taken (see Figure 2b). At the lowest speed (20 mV s⁻¹) the J–V curve displays hysteresis. In agreement with Figure 2a, the extended time spent around 7 V allows for ion detrapping which induces improved injection. This results in an increased current density in the returning sweep with respect to the forward sweep. This is not observed at the highest speed (400 mV s⁻¹) where the J–V curve displays a negligible hysteresis as well as low current density. The hysteresis and its dependence on sweep speed have been discussed in literature for a variety of different devices, generally referred to as memristive devices.[38]

As mentioned above, the drift direction of the ions is inverted by applying a negative bias. We decided to apply −2 V to avoid oxidation of the Al electrode (for 50 s). This permits the redistribution of ions at the electrodes and the filling of the cryptands throughout the device, resulting in a state of lower conductivity. Such state is probed performing a J–V sweep from 0 to 5 V at high speed (150 mV s⁻¹). Figure 2c displays such a measurement where the hysteresis is mostly suppressed and the maximum current density is in the order of 1 A m⁻². The process is reversible and the state of high conductivity is restored by applying 7 V (for 50 s). Figure 2d displays a J–V curve measured under the same conditions (0–5 V, 150 mV s⁻¹). In this case the curve displays the hysteresis described above and the current density increased by a factor of more than 40. During a J–V sweep to 5 V, devices without cryptand addition show a significantly increased current density (see Figure S4, Supporting Information). In devices with cryptand, remaining free ions are nonetheless mobile in the same voltage range, as displayed in Figure 2d. This suggests that the underlying injection mechanism, as described for LECs, is still valid for the here-presented device and the added cryptand solely stabilizes the ionic state.

For practical applications, probing the state of the device is achieved by measuring the current density upon applying a bias. The latter should be low enough to avoid influencing the trapped ions. From Figure 2a, we deduce 5 V to be a suitable working point, as the measured current density is stable over time. A custom voltage pulse train was designed in order to test the ability of setting and resetting the device between a high conductivity and low conductivity state, defined as an on and off state, respectively. The top part of **Figure 3**a displays the evolution of the applied bias over time, based on a four-step procedure: i) a 7 V bias (10 s) was first applied as a "write" operation, in order to set the device into its on-state, ii) a 5 V bias (1 s) was applied as a "read" operation, iii) a −2 V bias (10 s) was applied, in order to set the device into its off-state, followed by iv) a 5 V bias (1 s) "read" operation. The bottom part of Figure 3a

ADVANCED
SCIENCE NEWS
www.advancedsciencenews.com

ADVANCED
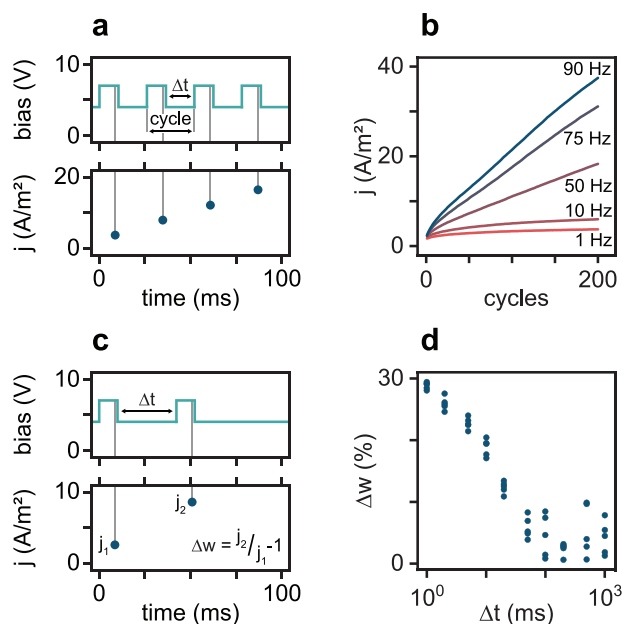**ELECTRONIC**
MATERIALS
www.advelectronicmat.de

Figure 3. a) Repeatable switching between on and off-state is tested by applying measurement cycles consisting of a write (7 V), read (5 V), erase (−2 V), and another read (5 V) operation in series. b) Stable current density values are measured for on and off-states over the course of 100 cycles. c) State retention is tested by applying a write (7 V) or erase (−2 V) operation followed by a continuous read (5 V) operation. d) Distinguishable states are retained over 300 s.

Figure 4. a) Frequency response is tested by applying pulsed cycles of varying frequency, consisting of a 10 ms pulse (7 V), followed by a variable interpulse time (4 V). b) With increasing frequency, a steeper increase in current density is observed over the course of 200 cycles. c) Two consecutive pulses (7 V) are applied with varying interpulse time with a baseline of 4 V and the relative weight change (Δw) is calculated. d) The relative weight increase correlates with decreasing interpulse time.

reports the measured current during the "read" operations. As expected, the on-state displays a higher current than the off-state (by a factor of 30). In order to show the repeatability of the device behavior, the four-step procedure was repeated 100 times. Figure 3b reports the current density measured for each "read" operation, demonstrating highly reliable behavior of the device.

An important parameter to be tested is the retention of the on and off-states. To test the retention of the on-state, the device was first biased at 7 V (30 s) as "write" operation and then biased at 5 V (300 s) as "read" operation. During the "read" operation, the current density was measured every second. The top part of Figure 3c schematically represents the applied bias (blue line); the bottom part represents the measured current (blue dots). Similarly, the retention of the off-state was tested by applying −2 V (30 s) as "erase" operation and then by applying a bias of 5 V (300 s) as "read" operation (see red line and dots in Figure 3c). The current density measured during the retention test for the on-state and for the off-state are reported in Figure 3d. A monotonic variation of the current density of each state is observed over time. This is due to ion movement induced by the constant 5 V applied during the test. Nonetheless both states remain distinguishable for more than 300 s, demonstrating the mid-term stability of the device.

Given the reproducibility and time-dependency of the electronic behavior, the two-terminal device shows characteristics as required for neuromorphic applications. In order to further investigate its time-dependent behavior, the device was tested with a square wave voltage signal. The latter consist of a 7 V

pulse (for 10 ms), followed by a "pause" phase at 4 V bias with a variable length (Δt). The current density was measured at the end of each 7 V pulse. The top part of **Figure 4**a displays the applied bias as a function of time (four cycles), while the bottom part indicates the current density measured at the end of each pulse. The drift of ions induced by the bias pulses is expected to gradually modify the ion distribution within the device, hence leading to a corresponding increase of current density, as explained above. By shortening the "pause" phase length (Δt), it is possible to increase the frequency of the square wave obtained in this way. Figure 4b reports the current density measured over 200 cycles for the different frequencies employed (between 1 and 90 Hz). A detailed list of frequencies, corresponding interpulse times and resulting root mean square voltages is listed in Figure S5 in the Supporting Information.

For a set frequency, the current density increases with the number of applied pulses. This behavior corresponds to a gradual modification of ion distribution, as previously described. Additionally, higher frequency leads to higher current density (for the same number of pulses). Since the "write" pulse remains consistent across all measurements, the variable "pause" phase must be responsible for the observed behavior. The lower bias of the "pause" phase (4 V), allows for ion diffusion to occur, thus partially resetting the device state. With increasing frequency, the length of this phase is shortened, thus decreasing the available diffusion time. As displayed in Figure 4b for the 1 and 10 Hz curve, a steady state is reached after a sufficient number of pulses. The steady state is reached because the ion diffusion process in the "pause" phase (4 V)

is in a dynamic equilibrium with the ion drift process of the applied pulses (7 V). For higher frequencies, the steady state is not reached during the measurement and the current density linearly increases with the number of pulses.

In order to better quantify the dynamic behavior, two pulses (7 V) with variable interpulse time (Δt at 4 V) were applied. The top half of Figure 4c depicts the applied bias scheme. The current density was measured at the end of each pulse (see bottom part of Figure 4c) and the relative weight change was calculated as $\Delta w = j_2 / j_1 - 1$. Figure 4d reports the relative weight change (Δw) as a function of interpulse time (Δt, logarithmically displayed). Five measurements were made for each value of Δt in order to observe statistical variations. The plot shows a steady decrease of Δw for increasing Δt up to 100 ms. Δw measures the relative variation between two consecutive states in time. The longer the time between the two pulses, the more ion diffusion occurs, hence, the smaller is the difference between the states. This can be quantified through the current density. This signal behavior is known as paired-pulse facilitation (PPF). PPF is a form of short-term synaptic plasticity, a feature of the biological synapse.[39] At large Δt, the ion diffusion time is long enough to revert the changes in ion distribution resulting from the first pulse. As a result, Δw is no longer dependent on Δt for all Δt above a certain threshold. For the chosen experimental parameters, this threshold for Δt is 100 ms.

Neuromorphic functionality has been demonstrated for the here-presented device. Further optimization can be achieved in various ways. Carrier injection, ion mobility and device stability can be modified by employing different electrode and polymer materials. Further modifications of the ion dynamics are possible using different cryptand molecules and salts. Additionally, the chemical structure of the polymer itself can be altered, allowing for fine tuning of the device parameters. This may also include the fixation of counter ions or the cryptand as polymer side chains, in order to have full control over material composition and prevent phase separation. Another interesting prospect may arise from the light emission capability of the LEC-based device. The combined application of electronic and light-based phenomena could be combined to enhance neuromorphic functionality.

3. Conclusion

We fabricated a two-terminal device in which an organic matrix—based on a TEG-PF mixed ionic-electronic conductor polymer—serves as the active layer for the conduction of Li$^+$ ions. The ionic conduction properties were modified by mixing in cryptand molecules, which have the ability to reversibly capture Li$^+$ ions. Given the finite ion drift velocity, applying a bias between the device terminals results in a dynamic modification of the ion concentration at the electrodes. This is manifested through the time modulation of current density. The time dependent behavior is observed in J–V measurements by changing the bias sweep speed as well as by preconditioning the device with constant voltages, prior to the measurements. The device displays highly reproducible behavior upon bias cycling as well as mid-term retention of the programmed conduction states.

Due to the reproducible time-dependent electronic behavior, the device shows features suitable for neuromorphic applications. This was experimentally demonstrated by the observation of frequency-dependent short-term plasticity as well as paired-pulse facilitation behavior. The polymeric nature and the ion-modulated current, combined with the simple two-terminal architecture of the here-presented organic synaptic diode, opens a range of appealing possibilities for to the fabrication of organic artificial neural networks.

4. Experimental Section

Sample Preparation: Glass substrates with prepatterned ITO electrodes (Psiotec) were cleaned by sonication in aqueous Hellmanex II solution, acetone and isopropanol. The surface was then treated for 5 min in an oxygen plasma. [2.2.2]-Cryptand and LiOTf were each dissolved in THF to yield solutions of 20 mg mL^{-1}. After 1 h of stirring at 40 °C, equal volumes of both solutions were added to TEG-PF. THF was added to yield a solution of 10 mg mL^{-1} TEG-PF, 2.5 mg mL^{-1} [2.2.2]-cryptand, and 2.5 mg mL^{-1} LiOTf. After 12 h of stirring at 40 °C, the solution was filtered through a 0.4 μm Nylon filter. Static spin-coating at 1000 rpm yielded a film of 200 nm thickness, as measured via profilometry (Bruker Dektak XT). Evaporation of 100 nm of aluminum was performed in a vacuum chamber (base pressure 5×10^{-6} mbar, evaporation rate 0.5 Å s^{-1}) employing a shadow mask. The resulting square electrodes have an area of 4 mm^2. The fabricated devices were encapsulated using commercially available resin (Ossila) and hardened under UV light.

Electrical Device Characterization: Electrical device characterization was performed using a Keithley 4200A-SCS parameter analyzer, equipped with two source-measure units (4200-SMU) and a two-channel pulse-measure unit (4225-PMU), connected to remote switching units (5225-RPM). Electrical connections were made using two probers with coaxial probe tips MPI Corporation. A total of 30 devices were characterized. For each device, functionality was tested by basic tests, consisting of an J–V sweep to 7 V and by sequentially applying a bias of 7 V and −2 V. Between devices, no significant variations occurred during these basic tests (see Figure S6, Supporting Information).

Supporting Information

Supporting Information is available from the Wiley Online Library or from the author.

Conflict of Interest

The authors declare no conflict of interest.

Data Availability Statement

The data that support the findings of this study are available in the supplementary material of this article.

Keywords

[1] J. D. Kendall, S. Kumar, *Appl. Phys. Rev.* **2020**, *7*, 011305.

[2] S. Goswami, S. Goswami, T. Venkatesan, *Appl. Phys. Rev.* **2020**, *7*, 021303.

[3] Y. Zhang, Z. Wang, J. Zhu, Y. Yang, M. Rao, W. Song, Y. Zhuo, X. Zhang, M. Cui, L. Shen, R. Huang, J. Joshua Yang, *Appl. Phys. Rev.* **2020**, *7*, 011308.

[4] A. E. Pereda, *Nat. Rev. Neurosci.* **2014**, *15*, 250.

[5] K. Kaneto, T. Asano, W. Takashima, *Jpn. J. Appl. Phys.* **1991**, *30*, L215.

[6] Y. van de Burgt, E. Lubberman, E. J. Fuller, S. T. Keene, G. C. Faria, S. Agarwal, M. J. Marinella, A. Alec Talin, A. Salleo, *Nat. Mater.* **2017**, *16*, 414.

[7] D. Ielmini, S. Ambrogio, *Nanotechnology* **2020**, *31*, 092001.

[8] R. Waser, M. Aono, *Nat. Mater.* **2007**, *6*, 833.

[9] S. Park, J. Noh, M. L. Choo, A. M. Sheri, M. Chang, Y. B. Kim, C. J. Kim, M. Jeon, B. G. Lee, B. H. Lee, H. Hwang, *Nanotechnology* **2013**, *24*, 384009.

[10] G. Ligorio, M. V. Nardi, N. Koch, *Nano Lett.* **2017**, *17*, 1149.

[11] C. D. Wright, Y. Liu, K. I. Kohary, M. M. Aziz, R. J. Hicken, *Adv. Mater.* **2011**, *23*, 3408.

[12] S. R. Nandakumar, M. Le Gallo, I. Boybat, B. Rajendran, A. Sebastian, E. Eleftheriou, *J. Appl. Phys.* **2018**, *124*, 152135.

[13] A. F. Vincent, J. Larroque, N. Locatelli, N. B. Romdhane, O. Bichler, C. Gamrat, W. S. Zhao, J. Klein, S. Galdin-Retailleau, D. Querlioz, *IEEE Trans. Biomed. Circuits Syst.* **2015**, *9*, 166.

[14] S. R. Kulkarni, D. V. Kadetotad, S. Yin, J. Seo, B. Rajendran, presented at *2019 26th IEEE Int. Conf. Electron., Circuits Syst. (ICECS)*, Genoa, Italy, 27–29 November 2019.

[15] T. Mikolajick, C. Dehm, W. Hartner, I. Kasko, M. J. Kastner, N. Nagel, M. Moert, C. Mazure, *Microelectron. Reliab.* **2001**, *41*, 947.

[16] S. Majumdar, H. Tan, Q. H. Qin, S. van Dijken, *Adv. Electron. Mater.* **2019**, *5*, 1800795.

[17] G. Liu, C. Wang, W. Zhang, L. Pan, C. Zhang, X. Yang, F. Fan, Y. Chen, R.-W. Li, *Adv. Electron. Mater.* **2016**, *2*, 1500298.

[18] J. S. Najem, G. J. Taylor, R. J. Weiss, M. S. Hasan, G. Rose, C. D. Schuman, A. Belianinov, C. P. Collier, S. A. Sarles, *ACS Nano* **2018**, *12*, 4702.

[19] S. Koner, J. S. Najem, M. S. Hasan, S. A. Sarles, *Nanoscale* **2019**, *11*, 18640.

[20] R. D. Costa, *Light-Emitting Electrochemical Cells*, Springer International Publishing, Cham, Switzerland **2017**.

[21] Q. Pei, G. Yu, C. Zhang, Y. Yang, A. J. Heeger, *Science* **1995**, *269*, 1086.

[22] J. M. Leger, S. A. Carter, B. Ruhstaller, *J. Appl. Phys.* **2005**, *98*, 124907.

[23] T. J. Mills, M. C. Lonergan, *Phys. Rev. B* **2012**, *85*, 035203.

[24] S. B. Meier, S. van Reenen, B. Lefevre, D. Hartmann, H. J. Bolink, A. Winnacker, W. Sarfert, M. Kemerink, *Adv. Funct. Mater.* **2013**, *23*, 3531.

[25] J. Xu, A. Sandstrom, E. M. Lindh, W. Yang, S. Tang, L. Edman, *ACS Appl. Mater. Interfaces* **2018**, *10*, 33380.

[26] S. van Reenen, P. Matyba, A. Dzwilewski, R. A. J. Janssen, L. Edman, M. Kemerink, *Adv. Funct. Mater.* **2011**, *21*, 1795.

[27] L. D. Bastatas, K. Y. Lin, M. D. Moore, K. J. Suhr, M. H. Bowler, Y. Shen, B. J. Holliday, J. D. Slinker, *Langmuir* **2016**, *32*, 9468.

[28] E. Zysman-Colman, J. D. Slinker, J. B. Parker, G. G. Malliaras, S. Bernhard, *Chem. Mater.* **2008**, *20*, 388.

[29] J. M. Lehn, J. P. Sauvage, *J. Am. Chem. Soc.* **1975**, *97*, 6700.

[30] G. Mauthner, U. Scherf, E. J. W. List, *Appl. Phys. Lett.* **2007**, *91*, 133501.

[31] Q. Pei, Yang, *J. Am. Chem. Soc.* **1996**, *118*, 7416.

[32] M. Grell, W. Knoll, D. Lupo, A. Meisel, T. Miteva, D. Neher, H.-G. Nothofer, U. Scherf, A. Yasuda, *Adv. Mater.* **1999**, *11*, 671.

[33] M. C. Lonergan, M. A. Ratner, D. F. Shriver, *J. Am. Chem. Soc.* **1995**, *117*, 2344.

[34] Z. Xue, D. He, X. Xie, *J. Mater. Chem. A* **2015**, *3*, 19218.

[35] F. P. Wenzl, C. Suess, P. Poelt, G. Mauthner, E. J. W. List, M. Bouguettaya, J. R. Reynolds, G. Leising, *Surf. Interface Anal.* **2004**, *36*, 1052.

[36] G. Mauthner, K. Landfester, A. Köck, H. Brückl, M. Kast, C. Stepper, E. J. W. List, *Org. Electron.* **2008**, *9*, 164.

[37] S. Sax, G. Mauthner, T. Piok, S. Pradhan, U. Scherf, E. J. W. List, *Org. Electron.* **2007**, *8*, 791.

[38] L. Chua, *Semicond. Sci. Technol.* **2014**, *29*, 104001.

[39] L. A. Santschi, P. K. Stanton, *Brain Res.* **2003**, *962*, 78.